Slowdown mechanisms of ultraintense laser propagation in critical density plasma

T. Iwawaki,[1] H. Habara,[1] T. Yabuuchi,[1,*] M. Hata,[2,†] H. Sakagami,[3] and K. A. Tanaka[1]
[1]*Graduate School of Engineering, Osaka University, Yamada-oka 2-1, Suita, Osaka 565-0871, Japan*
[2]*Department of Physics, Nagoya University, Nagoya, Aichi 464-8602, Japan*
[3]*Fundamental Physics Simulation Division, National Institute of Fusion Science, Toki, Gifu 509-5292, Japan*
(Received 16 July 2014; revised manuscript received 31 March 2015; published 27 July 2015)

We use one- and two-dimensional particle-in-cell simulations to demonstrate that the propagation of an ultraintense laser ($I = 10^{19}$ W/cm^2) in critical density plasma can be interfered with by a high density plasma wall region generated at the propagation front. When the electron flow speed of the wall region exceeds a certain relativistic threshold, the region behaves as an overdense plasma due to a decrease of the effective critical density. The region forms then very small overdense plasma islands. The islands impede the propagation intermittently and slow down the propagation speed significantly.

DOI: 10.1103/PhysRevE.92.013106 PACS number(s): 52.35.Mw, 52.27.Ny, 52.65.Rr, 52.38.Hb

The propagation of the ultraintense laser pulse (UILP) in plasmas is an important subject and has been studied for high energy density physics applications such as particle acceleration [1,2], x-ray production [3], and fast ignition [4]. When an UILP propagates in plasmas, the motion of electrons in the electromagnetic field becomes relativistic for laser intensity above 10^{18} W/cm^2 with its Lorenz factor $\gamma = \sqrt{1 + a_0^2/2} > 1$. Here a_0 is the normalized vector potential. The increased electron inertia decreases the plasma frequency, resulting in relativistic induced transparency [5] and relativistic self-focusing [6]. The UILP may propagate through a millimeter scale both underdense and overdense plasmas when the intensity is kept at above $I = 10^{18}$ W/cm^2 [7,8]. The propagation speed is defined by the balance of the incoming and reflecting lasers and electron kinetic energy [9]. The speed is slower than the simple group velocity. In this propagation, the discontinuity of plasma frequency at the pulse front acts as a moving mirror reflecting the UILP. The bifurcation and the density pileup at the pulse front may occur, related closely to the propagation speed of the UILP. Both moving mirror and piled up electrons may contribute to the slowdown of the propagation. However, in depth analysis of the interactions is lacking [7–9].

In this study, using one-dimensional (1D) and 2D particle-in-cell (PIC) simulations, we describe the UILP behaviors in a critical density plasma and find a different mechanism of the UILP deceleration. During the laser propagation, the piled up wall region at the front of the UILP is accelerated to have a relativistic flow speed v_r by the ponderomotive force (PMF). The flow speed appears to decrease the frequency of the incoming laser with respect to the piled up wall region due to the Doppler effect. This downshift decreases also the effective critical density with the region accordingly. When the effective critical density decreases significantly, the UILP may experience the plasma as overdense and be reflected from this piled up wall region. Then multiple small overdense regions (islands) are created. These collective interactions may result in the significant slowdown of the propagation speed. We derive first the effective critical density including the Doppler effect. Considering a one-dimensional coordinate, the frequency and the wave number of the incident laser become $\omega'_L/\omega_L = (1 - \beta_r/\beta_\phi)/\gamma_r(1 - \beta_r^2)$ and $k'_L/k_L = (1 - \beta_r\beta_\phi)/\gamma_r(1 - \beta_r^2)$ at the piled up wall region frame. Here k_L and β_ϕ are, respectively, the wave number and the phase speed of light normalized with that in vacuum in the rest frame with $\beta_r = v_r/c$. The phase speed is expressed as $\beta_\phi = 1/\sqrt{1 - N_e/N_c\gamma_f}$, where γ_f, N_e, N_c, and γ_r are the electron Lorentz factor in the rest frame, the electron density, the classical critical density, and the Lorenz factor of the flow speed, respectively. Substituting the above relations into the dispersion relation of electromagnetic waves in plasmas at the wall frame $\omega'^2_L - c^2k'^2_L - \omega_p^2/\gamma' = 0$, we obtain the effective critical density

$$N_{ec} = \gamma' \frac{(1 - \beta_r/\beta_\phi)^2}{1 - \beta_r^2} N_c. \tag{1}$$

Here γ' is the electron Lorenz factor at the wall frame; $\gamma' = \sqrt{1 + a_0'^2/2}$ is valid for a linearly polarized light, where the laser vector potential is transformed to be $a'_0/a_0 = (1 - \beta_r/\beta_\phi)/(1 + \beta_r)$ at the wall frame. When the flow speed β_r increases, the N_{ec} decreases as shown in Fig. 1. This figure is based on the calculation using Eq. (1) and shows the effective critical density as a function of the flow speed when the plasma density and the laser intensity are classical critical and 10^{19} W/cm^2. Using the above relations, we can estimate a threshold flow speed of the piled up wall region that can make the region effectively overdense plasma. When the incident laser intensity is 10^{19} W/cm^2 ($a_0 = 2.8$) and the background electron density is classical critical, the threshold flow speed is estimated to be $\beta_r = 0.31$.

We proceed to see how the piled up wall region at the front becomes effectively overdense using a 1D PIC simulation (FISCOF1 [10]). In this simulation, the initial plasma has a uniform electron density profile with the classical critical density. The ions consist of mobile protons. The mass ratio of the ion to the electron is 1836. The grid resolution is 0.044 μm and 100 particles per cell are used for each species. The initial temperatures of electrons and ions are set to be 10 keV. This

*Present address: RIKEN SPring-8 Center, 1-1-1 Kouto, Sayo-cho, Sayo-gun, Hyogo 679-5148, Japan.
†Present address: Institute of Laser Engineering, Osaka University, Yamada-oka 2-6, Suita, Osaka 565-0871, Japan.

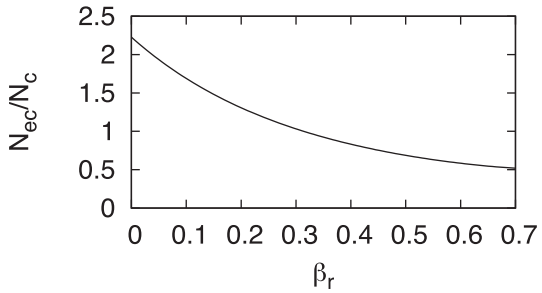

FIG. 1. Effective critical density as a function of the flow speed (normalized with the speed of light). Here the plasma density and the laser intensity are classical critical and 10^{19} W/cm^2, respectively.

plasma starts at 0 μm toward the right up to 500 μm and a vacuum region toward the left up to 100 μm. The plasma density rises sharply from 0 to classical critical at 0 μm. The input laser ($\lambda = 1$ μm) comes from the vacuum and propagates into the plasma region with a rise time of 10 fs (Gaussian). After the rise, the intensity is kept constant at 10^{19} W/cm^2.

When the UILP penetrates the plasma, the plasma frequency is decreased. Figure 2(a) shows spatial distributions of the electron density (plasma frequency) normalized by the relativistic critical density $N_{cr} = \gamma N_c$ (black line) and the laser intensity normalized by the input intensity I_0 (gray line) at 50 fs. These values are time averaged within the laser period $2\pi/\omega_L$. The discontinuity at the front (moving mirror) created by the relativistic effect is observed around 8.5 μm in Fig. 2(a). The moving mirror speed obtained is $0.42c$, although the simple group velocity derived from the dispersion relation $v_g = 0.73c$. Here we used $v_g = c\sqrt{1 - N_e/\gamma N_c}$, $N_e = N_c$, and $\gamma = \sqrt{1 + a_0^2/2}$. This observed propagation speed agrees well with that derived from the formula using the energy balance $0.45c$ [9].

When the incident laser is reflected by the mirror, the PMF accelerates electrons at the mirror in the forward direction and piles up electrons at the mirror. Figure 2(b) shows spatial distributions of the electron density normalized by the classical critical density (black line) and the electron flow speed (gray line). These values are also time averaged within the laser period. The flow speed is defined as a speed averaged among all electrons within a grid. The piled up wall region is observed around 8.5 μm. The peaks of electron density and flow speed of the region are $1.32N_c \pm 0.02N_c$ and $0.09c$, respectively. Using the flow and the phase speeds inside the laser pulse, the effective critical density of the wall region is estimated to be $1.70N_c \pm 0.02N_c$ and the threshold flow speeds is estimated to be $0.17c$ using Eq. (1). Considering that the effective critical density is higher than the electron density of the wall (the threshold speed is faster than the flow speed), the wall is underdense for the incident laser. Therefore, the incident laser is able to penetrate the wall region and increase the relativistic critical density of the region via relativistic effect.

The intermittent acceleration and deceleration of the flow speed take place when the piled up wall region absorbs the Langmuir waves. The Langmuir wave may have positive (forward) and negative (backward) components. When the incident laser is reflected by the moving mirror, the oscillating component in the PMF $2\omega'_L$ pushes electrons forward at the mirror periodically and excites the Langmuir waves [11]. The group velocity $v_{gL} = (1/2)\sqrt{3/2}(\omega_p/\omega'_L)v_{th}\sqrt{(2\omega'_L/\omega_p)^2 - 1}$ is derived from the dispersion relation $4\omega_L'^2 = \omega_p^2 + 3k^2v_{th}^2/2$. In this simulation, the group velocity is close to the electron thermal velocity $v_{gL} \sim v_{th}$. Using the relation $v_{th} = \sqrt{2T_e/m_e}$, the group velocity of the wave becomes faster than the propagation speed of the laser when the temperature is over 50 keV. The plasma ahead of the mirror is actually heated immediately up to over 50 keV by the UILP and then the temperature decreases to 10 keV or so in the forward direction away from the mirror position. The excited wave propagates and gains energy. Figure 3(a) shows spatial distributions of the laser

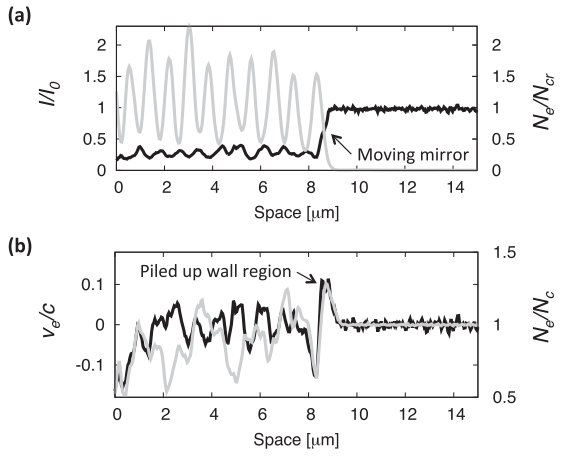

FIG. 2. (a) The black and gray lines show the spatial distributions of the electron density normalized by the relativistic critical density and the laser intensity normalized by the input laser intensity at 50 fs. (b) The black and gray lines show the spatial distributions of the electron density normalized by the classical critical density and the electron flow speed at 50 fs.

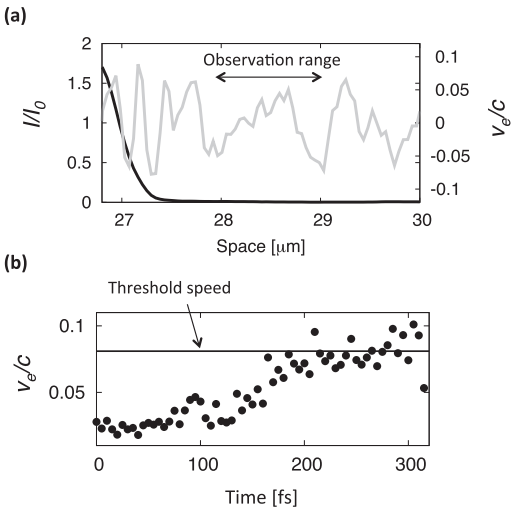

FIG. 3. (a) The black and gray lines show spatial distributions of the laser intensity and the instantaneous flow speed at 200 fs. (b) The maximum flow speed ahead of the UILP as a function of time. The solid line at the maximum flow speed $0.08c$ shows the threshold flow speed for the effective critical density at the piled up region.

intensity (black line) and the instantaneous electron flow speed (gray line) at 200 fs. The induced Langmuir wave is observed ahead of the front. Figure 3(b) shows the maximum flow speed taken between 1 and 2 μm ahead of the propagation front as a function of time. The speed increases in time from an initial $0.02c$ to more than $0.1c$ at 380 fs due to an increase of the wave energy. Due to this speed increase, it is observed that the flow keeps absorbing the Langmuir waves. Considering that the threshold flow speed of the piled up wall region is $0.17c$ as mentioned above, the region becomes effectively an overdense plasma after the waves have flow speed above $0.08c$ since the initial flow speed of the region is $0.09c$. The time required to reach the threshold is about 300 fs, as shown in Fig. 3(b). After 300 fs, the effective critical density decreases more drastically based on Eq. (1) and the region becomes effectively overdense. The piled up electrons are able now to reflect the incident laser.

This reflection from the piled up region can be confirmed also by observing the reflected light spectrum. When the incident laser is reflected, the reflected light should show a Doppler shift. Using the Doppler shift relation $\omega_L''/\omega_L = (1+\beta_p^2-2\beta_p/\beta_\phi)/(1-\beta_p^2)$, the speed of the reflector β_p can be estimated. The black line in Fig. 4(a) indicates the reflected spectrum between 300 and 900 fs. The observed spectrum has peaks around $0.56\omega_L$ and $0.72\omega_L$. Using the phase velocity β_ϕ (1.13), the reflector speed β_p at $0.72\omega_L$ becomes $0.19c$. This speed is in good agreement with the threshold wall speed ($0.17c$). This component around $0.72\omega_L$ is not observed between 0 and 200 fs indicated by the gray line. Here we note that the speed at $0.53\omega_L$ corresponds to the propagation speed ($0.42c$) in the early time. This result indicates that the plasma of the wall region becomes effectively overdense and reflects the incident laser after 300 fs.

Now we look into the detailed behaviors of the UILP interaction with the wall region. Considering that the thickness of the region is shorter than the wavelength of the incident laser as shown by the black line in Fig. 2(b), a portion of the laser intensity transmits the region and piles up other electrons in the deeper region of the plasma. If the flow speed of another one exceeds the threshold, the piled up region also becomes effectively overdense and reflects the laser. These mechanisms affect the laser propagation incessantly around the front position of the UILP. Figure 4(b) shows the spatial distribution of the electron density normalized by the effective critical density shown as Eq. (1) (black line) and the laser intensity (gray line) at 400 fs. Multiple small overdense regions (islands) generated from the wall region are observed around 47 μm.

We now estimate how these islands influence the laser propagation. The interaction can be described by the scattering theory approximately using the Dirac δ function. Assuming the laser vector potential at the moving frame $a'(x',t') = a'(x')\exp(i\omega' t')$, the equation is

$$\left[\frac{d^2}{dx'^2}+\kappa^2+g^2\delta(x')\right]a'(x')=0. \tag{2}$$

Here $\kappa^2=\omega'^2/c^2-\omega_{eb}^2/c^2\gamma_b$ and $g=\lambda_i'(\omega_{ei}^2/\gamma_i-\omega_{eb}^2/\gamma_b)/c^2$ within $\gamma_r \ll \gamma_b$ and $\gamma_i' \sim \gamma_i$, where ω_{eb} and γ_b are the background plasma frequency and Lorenz factor, respectively, and ω_{ei}, λ_i', and γ_i are the plasma frequency, the plasma length, and the Lorenz factor of the island, respectively. Assuming that the vector potentials are $a'(x')=\exp(i\kappa x')+\rho\exp(-i\kappa x')$ in front of the island and $a'(x')=\tau\exp(i\kappa x')$ after passing the island, we obtain the transmittance $T=4\kappa^2/(4\kappa^2+g^2)$ and the reflectance $R=g^2/(4\kappa^2+g^2)$. Using these relations and spatial distributions of the electron density normalized by the effective critical density, we calculate the front position of the laser pulse at each time. In the calculation, the input laser comes from the vacuum region. When the laser arrives at the effective overdense plasma, T and R are calculated. Using these calculated values, we estimate the spatial distributions of the laser intensity and the front positions. Figure 5 shows the front position as a function of time. The results (triangles) agree well with the PIC results (circles). Considering that the estimated front position including the islands effectively reproduces the PIC simulation, the laser propagation is impeded by the islands after 350 fs. This slowdown is also

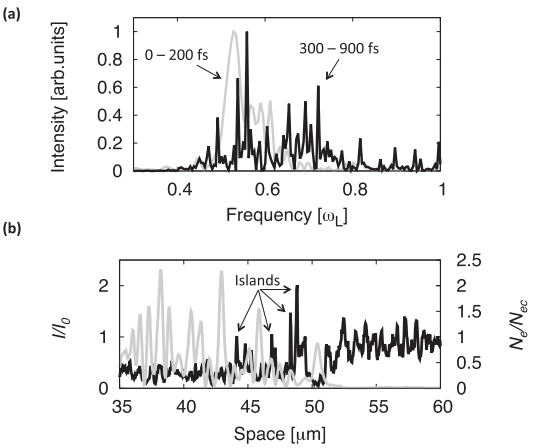

FIG. 4. (a) Frequency spectra of the reflected light. Observed periods in black and gray lines are between 0 and 200 fs and 300 and 900 fs, respectively. (b) The black and gray lines indicate the spatial distribution of the electron density normalized by the effective critical density and the laser intensity at 400 fs.

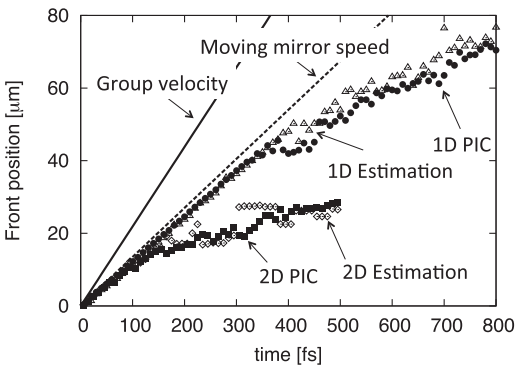

FIG. 5. Time development of the front position. The position is defined as the furthest through the plasma at which the intensity keeps the initial value I_0. Closed circles, triangles, closed squares, and diamonds show the results of the 1D PIC simulation, the estimation in one dimension, the 2D PIC simulation, and the estimation in two dimensions, respectively. The solid line is the result of the group velocity $v_g = 0.73c$. The dashed line is the result of the moving mirror speed derived from the formula [9].

observed in various laser intensities (0.5–10) $\times 10^{19}$ W/cm^2 and the speed is expressed as $v_s = \exp\{-[5 - \ln(I_{20})]^2/30\}c$, where I_{20} is the laser intensity in units of 10^{20} W/cm^2. Here we note that this slowdown speed and timing do not depend on the ion inertia.

More realistic behavior can be understood by using a 2D PIC simulation. Here we use a 2D PIC code FISCOF2 [10]. The simulation setup is also the same as the 1D case except with the laser spot size (7 μm, Gaussian shape) and the transverse and horizontal lengths of the plasma (30 and 60 μm). Particles and fields are set to be absorbed at the boundary. This boundary condition does not influence the laser propagation because the transverse length of the plasma is much larger than the laser spot size. The front position from the simulation is plotted as closed squares in Fig. 5. Despite the laser propagating with the same speed as the result from the 1D PIC simulation until 50 fs, the slowdown is observed much earlier in time than that in the 1D case. To understand this early slowdown in two dimensions, we calculate the front position along the center axis of the laser spot using the same analysis as in the 1D case. The results are shown as diamonds in Fig. 5, which show good agreement with the 2D simulation (squares). Now we can discuss further the slowdown time between the 1D and 2D cases using an analytical estimation. The peaks of the electron density and flow speed of the wall region at between 0 and 50 fs are estimated to be $1.42N_c \pm 0.03N_c$ and $0.15c \pm 0.01c$, respectively. This speed is about 2 times higher than in the 1D case, whereas the density increase is only 10%. That makes the wall region more unstable than in the 1D case, resulting in the generation of islands in early time. Here we note that the difference in the flow speed can be explained by the forward moving and return currents [12]. Figures 6(a) and 6(b) show the spatial distributions of the electron density normalized by the effective critical density at 40 and 50 fs. The laser intensity plots are shown in Figs. 6(c) and 6(d). An island around the front is observed in Fig. 6(a) at $X = 4$ μm and in Fig. 6(b) at $X = 6$ μm. The other two islands around $X = 2.5$ μm in Fig. 6(a) are generated by filaments of the laser indicated in Fig. 6(c). The laser propagation before reaching the very front keeps the channel temperature rather high (~2 MeV) and suppress the filamentation instability. However, when the laser pulse meets a fresh plasma at the very front, the plasma temperature is still cool (~50 keV) and helps increase the filamentation growth rate [13]. These divided filaments propagate at an angle with speed depending on each intensity. When the piled up regions at the fronts become effectively overdense, islands are generated from the walls as shown Fig. 6(a). These islands interrupt the energy supply for further propagations, resulting in the decrease of the laser intensity around the front position at the later time as shown Fig. 6(d). While the weakened pulse at the front tries to propagate further, another island can be created as shown in Fig. 6(b). The process destabilizes the propagation especially at the front region and decelerates the propagation speed from $0.42c$ to $0.14c \pm 0.01c$. Even if some other mechanisms such as self-focusing, diffraction, or bifurcation are involved in the laser propagation, this process occurs no matter what parameters are used in the simulation since the interaction physics at the piled up wall region stays the same. However, the v_s that the results of 1D PIC simulations indicate that the islands' interruption will be reduced when the self-focusing that enforces the laser intensity dominates the laser propagation.

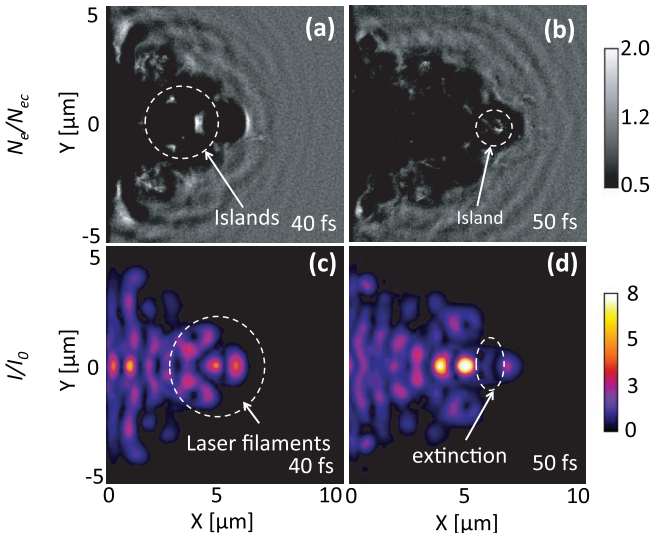

FIG. 6. (Color) Electron density normalized by the (a) and (b) effective critical density and (c) and (d) laser intensity at 40 and 50 fs.

Although the laser energy could escape to another direction in the 2D case from the propagation axis, the bifurcation does not take place effectively and the interaction with the islands reduces heavily the laser intensity. This is because the islands are generated from the piled up wall at the front and the size of the island is of the same order as the diameter of the plasma channel or filaments. If islands are created by other mechanisms and the size is smaller than the plasma channel, the single laser pulse propagating in the plasma could be bifurcated by the island.

In this study, we clarified the propagation of the ultraintense laser in a classical critical density plasma. At the beginning of the propagation, the moving mirror is formed as a result of the discontinuity structure due to the plasma frequency jump. Then a piled up wall region is created via the ponderomotive force. When the flow speed of the region exceeds a certain threshold, the region acts as an overdense plasma due to a decrease of the effective critical density at the region with the aid of the Doppler effect. The overdense piled up region reflects the incident laser and generates high density islands. The islands interrupt the following laser propagation and finally the propagation speed is significantly decelerated to $0.14c$ in two dimensions from $0.73c$ based on the simple dispersion relation.

This work is supported in part by the Grants-in-Aid for Scientific Research (A) (Grant No. 22246122) and (B) (Grant No. 23360412) from the Japan Society for the Promotion of Science (JSPS) of Japan. T.I. is supported by the Research Fellowship (Grant No. 25.858) from the JSPS of Japan. Part of this research was supported by the x-ray free electron laser priority strategy of MEXT (012005014 Osaka University).

[1] J. Faure, Y. Glinec, A. Pukhov, S. Kiselev, S. Gordienko, E. Lefebvre, J.-P. Rousseau, F. Burgy, and V. Malka, Nature (London) **431**, 541 (2004).

[2] T. Schlegel, N. Naumova, V. T. Tikhonchuk, C. Labaune, I. V. Sokolov, and G. Mourou, Phys. Plasmas **16**, 083103 (2009).

[3] S. V. Bulanov, T. Esirkepov, and T. Tajima, Phys. Rev. Lett. **91**, 085001 (2003).

[4] M. Tabak, J. Hammer, M. E. Glinsky, W. L. Kruer, S. C. Wilks, J. Woodworth, E. M. Campbell, M. D. Perry, and R. J. Mason, Phys. Plasmas **1**, 1626 (1994).

[5] P. Kaw and J. Dawson, Phys. Fluids **13**, 472 (1970).

[6] C. E. Max, J. Arons, and A. B. Langdon, Phys. Rev. Lett. **33**, 209 (1974).

[7] G. Li, R. Yan, C. Ren, T. L. Wang, J. Tonge, and W. B. Mori, Phys. Rev. Lett. **100**, 125002 (2008).

[8] L. Willingale, P. M. Nilson, A. G. R. Thomas, S. S. Bulanov, A. Maksimchuk, W. Nazarov, T. C. Sangster, C. Stoeckl, and K. Krushelnick, Phys. Plasmas **18**, 056706 (2011).

[9] S. Guérin, P. Mora, J. C. Adam, A. Héron, and G. Laval, Phys. Plasmas **3**, 2693 (1996).

[10] H. Sakagami and K. Mima, in *Proceedings of the Second International Conference on Inertial Fusion Sciences and Applications*, edited by K. Tanaka *et al.* (Elsevier, Paris, 2001), p. 380.

[11] H. Sakagami and K. Mima, Phys. Rev. E **54**, 1870 (1996).

[12] Y. Sentoku, K. Mima, P. Kaw, and K. Nishikawa, Phys. Rev. Lett. **90**, 155001 (2003).

[13] W. L. Kruer, in *The Physic of Laser Plasma Interactions*, edited by D. Pines (Westview, Boulder, 2003), Chap. 8, pp. 93–94.